Solar Energy Materials & Solar Cells 158 (2016) 50–54

Contents lists available at ScienceDirect

Solar Energy Materials & Solar Cells

journal homepage: www.elsevier.com/locate/solmat

21.0%-efficient screen-printed *n*-PERT back-junction silicon solar cell with plasma-deposited boron diffusion source

Nadine Wehmeier [a,*], Anja Nowack [a], Bianca Lim [a,1], Till Brendemühl [a], Sarah Kajari-Schröder [a], Jan Schmidt [a,b], Rolf Brendel [a,b], Thorsten Dullweber [a]

[a] Institute for Solar Energy Research Hamelin (ISFH), Am Ohrberg 1, 31860 Emmerthal, Germany
[b] Department Solar Energy, Institute of Solid-State Physics, Leibniz University Hanover, Appel Str. 2, 30167 Hanover, Germany

ARTICLE INFO

Article history:
Received 28 March 2016
Received in revised form
20 May 2016
Accepted 23 May 2016
Available online 18 June 2016

Keywords:
Silicon solar cells
n-PERT back junction
PECVD boron silicate glass
Co-diffusion
Device simulation
Efficiency gain analysis

ABSTRACT

The manufacturing process of Passivated Emitter and Rear Totally diffused (PERT) solar cells on *n*-type crystalline silicon is significantly simplified by applying multifunctional layer stacks acting as diffusion source, etching and diffusion barrier. We apply boron silicate glasses (BSG) capped with silicon nitride (SiN_z) layers that are deposited by means of plasma enhanced chemical vapor deposition (PECVD). Optimum PECVD deposition parameters for the BSG layer such as the gas flow ratio of the precursor gases silane and diborane $SiH_4/B_2H_6=8\%$ and the layer thickness of 40 nm result in a boron diffusion with saturation current density $J_{0,B}$ below 10 fA/cm^2 applying an AlO_x/SiN_y passivation and firing. The PECVD BSG diffusion source is integrated into the *n*-type PERT back junction (BJ) solar cell process with screen-printed front and rear contacts. The only high temperature step is a $POCl_3$ co-diffusion for the formation of the boron emitter from the PECVD BSG layer and for the formation of the phosphorus-doped front surface field (FSF). An independently confirmed energy conversion efficiency of 21.0% is achieved for a 156×156 mm^2 large *n*-PERT BJ cell with this simplified process flow. This is the highest efficiency reported for a large-area co-diffused *n*-type PERT BJ solar cell using a PECVD BSG as diffusion source. For comparison, reference *n*-type PERT BJ cells with separate $POCl_3$ and BBr_3 diffusions reach an efficiency of 21.2% in our lab. A synergistic efficiency gain analysis (SEGA) for the co-diffused *n*-PERT BJ cell shows that the main possible efficiency gain of 1.1%$_{abs.}$ originates from recombination in the phosphorus-diffused front surface field while the PECVD BSG boron-doped emitter accounts for only 0.1%$_{abs.}$ efficiency gain. We evaluate the use of the PECVD BSG/SiN_z stack as a rear side passivation as a replacement of the AlO_x/SiN_y stack in order to further simplify the process flow. We obtain $J_{0,B}$ values of 40 fA/cm^2, an implied open-circuit voltage of 682 mV and a simulated *n*-PERT BJ cell efficiency of 21.1%.

1. Introduction

The Passivated Emitter and Rear Cell (PERC) concept on *p*-type silicon wafers is expected to become a major industrial solar cell technology [1]. With a lean process flow, efficiencies of up to 22.1% [2] were recently demonstrated. However, the efficiency of PERC solar cells typically decreases around 0.5%$_{abs}$ due to light-induced degradation (LID) of the boron-doped *p*-type Czochralski-grown (Cz) silicon used as base material [3,4].

Fig. 1 shows an *n*-type silicon PERT (*n*-PERT) BJ cell. This is an attractive cell concept which combines the advantages of *n*-type silicon (no LID, high bulk lifetime [5]) and of a process flow that is very similar to industrial *p*-type PERC (*p*-PERC) cells. The PERT BJ fabrication has the potential to be further simplified and to be implemented in existing PERC production lines. Until now, *n*-PERT BJ cells applying BBr_3 and $POCl_3$ furnace diffusions have demonstrated conversion efficiencies up to 22.5% using Ni/Cu/Ag plating on the front side and AlSi sputtering on the rear side for metallization [6] and with screen-printed contacts up to 21.4% [7] and very recently of 21.8% [8]. In this work, we apply plasma enhanced chemical vapor deposition (PECVD) of boron silicate glass (BSG). Combined with a co-diffusion process, this is an alternative approach to introduce the rear side p^+-emitter and the n^+-front surface field (FSF) of the *n*-PERT BJ cells. As an approach for process simplification, CVD BSG layers combined with a $POCl_3$ co-diffusion have already been applied to *n*-PERT solar cells (front and back junction) [9–11] reaching conversion efficiencies up to 19.9%

* Corresponding author.
E-mail address: wehmeier@isfh.de (N. Wehmeier).
[1] Now with the Solar Energy Research Institute of Singapore, National University of Singapore, 117574, Singapore.

http://dx.doi.org/10.1016/j.solmat.2016.05.054
0927-0248/

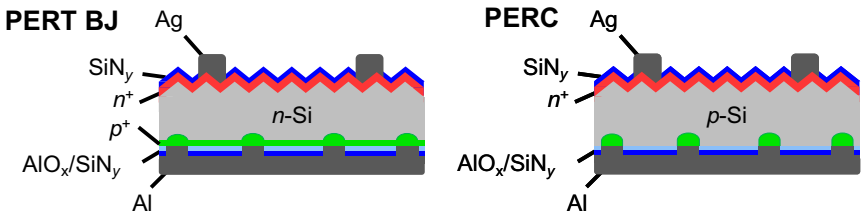

Fig. 1. Schematic diagram of the *n*-PERT BJ cell compared to the *p*-PERC cell.

[9] and 20.1% for bifacial devices [11].

We demonstrate monofacial *n*-PERT BJ cells with a record-high conversion efficiency of 21.0% with a co-diffused boron emitter from a PECVD BSG/SiN_z stack that has already been presented in [12]. In this paper, we show a SEGA for the best *n*-PERT BJ cell that proves the high quality of the PECVD BSG diffusion source and shows the highest potential for synergistic cell improvements of up to 4.1%$_{abs.}$ by eliminating recombination, especially in the P FSF.

To further simplify the process, the multifunctional use of PECVD stacks as diffusion source and also as rear side passivation instead of AlO_x/SiN_y has been proposed and J_0 values down to 50 fA/cm^2 have been demonstrated for a BSG/SiN_x passivation by Engelhardt et al. [13]. In this work, we investigate the passivation quality of BSG/SiN_z and BSG/SiO_xN_y stacks reaching lowest published J_0 results of 40 fA/cm^2 and evaluate the implementation in *n*-PERT BJ cell processing by device simulations.

2. Material and methods

2.1. PECVD layer stack and co-diffusion

The PECVD BSG deposition is performed in a cluster system (CS 400P, von Ardenne) with an inductively coupled plasma (ICP) source. For the deposition of a 20–120 nm thin BSG layer, we use the precursor gases silane (SiH_4), nitrous oxide (N_2O), and diborane (3% B_2H_6, diluted in 97% H_2). The ratio SiH_4/B_2H_6 is varied from 4% to 8%. For this calculation the B_2H_6 gas flow including the 97% H_2 dilution is used.

As a capping layer, we apply either a silicon nitride (SiN_z) (SiNA, Meyer Burger) with a thickness of 120–180 nm or a silicon oxynitride (SiO_xN_y) with a thickness of 200–300 nm. The SiO_xN_y layer is deposited in the same ICP deposition chamber as the BSG layer without breaking the vacuum. It has a higher etching rate in HF compared to SiN_z.

For the boron drive-in from the BSG layer, we apply a two-stage co-diffusion process in a $POCl_3$ furnace as described in [14] and as shown in Fig. 2: In one high-temperature process, the B drive-in from the PECVD BSG is performed first in an N_2 ambient at 950 °C for 60 min, and then a $POCl_3$ diffusion is applied at 829 °C. During the co-diffusion, the capping layer functions as a diffusion barrier against phosphorus. When an uncapped PECVD BSG layer is exposed to co-diffusion, a P in-diffusion disturbs the boron emitter formation as reported in [15].

2.2. Solar cell processing

For the processing of co-diffused *n*-PERT BJ cells as described in [12], 156 × 156 mm^2 phosphorus-doped *n*-type Cz silicon wafers with (100) orientation, a starting thickness of (180 ± 20) μm and a resistivity of 5–6 Ω cm after high-temperature treatment (T ≥ 950 °C) during the subsequent process flow are used. They are etched in KOH for saw damage removal and are subsequently RCA-cleaned. A 40 nm-thick PECVD BSG layer with a gas flow ratio of SiH_4/B_2H_6=8% is deposited on the planar rear side and capped

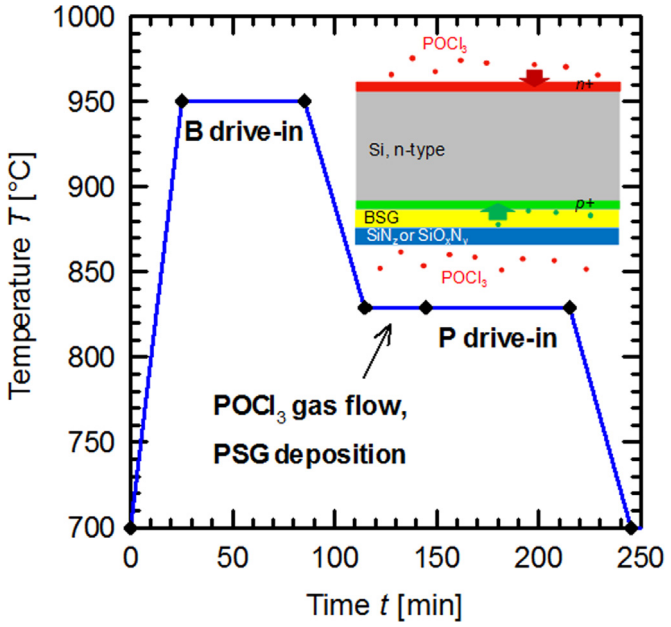

Fig. 2. Temperature profile of the two-stage co-diffusion [14]. The B drive-in from the PECVD BSG layer is performed at 950 °C in N_2 ambient. In the same high temperature process, a $POCl_3$ diffusion is performed at 829 °C. The BSG layer is capped with a PECVD SiN_z or SiO_xN_y layer to prevent P indiffusion.

with a 170 nm-thick PECVD SiN_z layer (SiNA, Meyer Burger). The thickness of the SiN_z layer is reduced during the following cleaning and etching steps, thus the higher thickness of 170 nm is chosen to ensure that the PECVD BSG/SiN_z stack acts as an etch barrier during the following alkaline texturing and as a diffusion barrier during the $POCl_3$ co-diffusion. After removal of all dielectric layers in HF, the rear side is passivated by a stack of 5 nm AlO_x deposited by spatial atomic layer deposition (ALD) (InPassion LAB tool, SoLayTec) and 100 nm SiN_y. On the front side, a PECVD SiN_y layer acts as passivation and as anti-reflecting coating (ARC). After laser contact opening on the rear side, the front side metallization is performed by Ag-screen printing applying a 5 busbar layout and a dual print process as described in [16]. Full-area Al-screen-printing on the rear side and co-firing finalize the cell as sketched in Fig. 1. For comparison, *n*-PERT BJ reference cells using sequential BBr_3 and $POCl_3$ diffusions are also fabricated as described in [17].

3. Results and discussion

3.1. Diffusion source and boron emitter

In order to characterize the boron emitter on planar *n*-type Cz-Si that is diffused from the PECVD BSG, we measure the boron sheet resistance $R_{sheet,B}$ by means of four point probe (FPP) (Polytec, 4Dimensions) after removal of all dielectric layers. We perform lifetime measurements using a Sinton lifetime tester on symmetrically boron diffused test structures after AlO_x/SiN_y

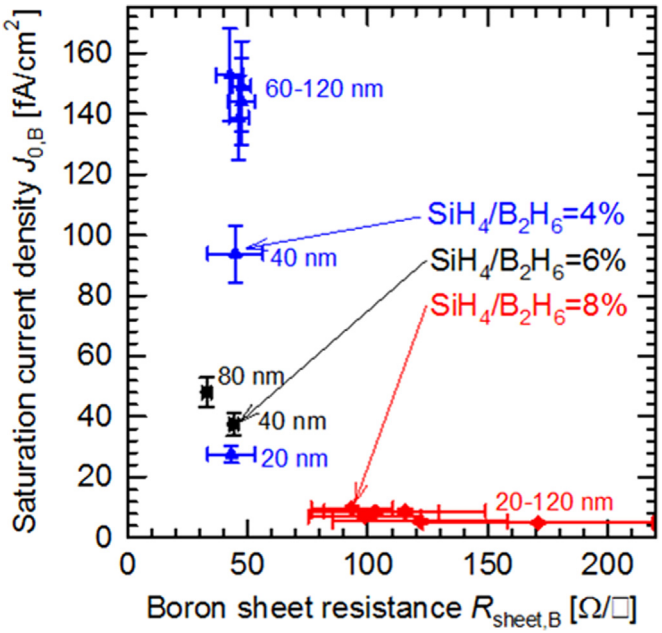

Fig. 3. Saturation current density $J_{0,B}$ and sheet resistance $R_{sheet,B}$ of the boron diffusion measured on symmetrically diffused and AlO_x/SiN_y passivated 156×156 mm^2 wafers after firing. $J_{0,B}$ and $R_{sheet,B}$ are influenced by the gas flow ratio SiH_4/B_2H_6 and the PECVD BSG thickness [12]. (For interpretation of the references to color in this figure, the reader is referred to the web version of this article.)

passivation and firing. The emitter saturation current density $J_{0,B}$ is extracted by applying the method by Kane and Swanson [18] using an intrinsic carrier concentration of $n_i = 8.6 \times 10^9$ cm^{-3}. The measured $J_{0,B}$ and $R_{sheet,B}$ are shown in Fig. 3 where every data point corresponds to the average value measured on a 156×156 mm^2 wafer area and the error bars correspond to the standard deviation.

The SiH_4/B_2H_6 gas flow ratio strongly influences $R_{sheet,B}$ and $J_{0,B}$ of the resulting boron diffusion, as discussed in detail in [14]. The PECVD BSG layer thickness has no discernible impact on the resulting $R_{sheet,B}$ but affects $J_{0,B}$, as shown in [12]: For the highest gas flow ratio of 8% (red diamonds) we measure a minimum saturation current density of (4.9 ± 0.5) fA/cm^2 and $J_{0,B}$ values below 10 fA/cm^2 for all PECVD BSG thicknesses and for a minimum boron sheet resistance of (93 ± 17) Ω/□. We attribute the increased $R_{sheet,B}$ of (171 ± 48) Ω/□ with a high standard deviation to an insufficient boron diffusion from the 20 nm-thin BSG layer. For the highest BSG thickness of 120 nm, we also observe an increased standard deviation of the sheet resistance $R_{sheet,B} = (122 \pm 36)$ Ω/□ that we attribute to an inhomogeneity in the thickness of the PECVD layer. For the lowest gas flow ratio of 4% (blue triangles) the saturation current density increases with increasing PECVD layer thickness while $R_{sheet,B}$ is approximately constant. We assume that for $SiH_4/B_2H_6 < 8\%$ a boron rich layer (BRL) is formed at the BSG-Si interface. The BRL formation is enhanced for thicker BSG layers and its presence lowers the surface quality and the lifetime properties [19] and thus increases the saturation current density.

From the measurement results shown in Fig. 3 we conclude that for an optimized boron diffusion source, a SiH_4/B_2H_6 gas flow ratio of 8% and a PECD BSG layer thickness of 40 nm shall be used so that boron emitters with $J_{0,B}$ values below 10 fA/cm^2 and $R_{sheet,B}$ below 100 Ω/□ can be reached with an AlO_x/SiN_y passivation while a BRL formation is avoided.

3.2. BSG/SiN$_z$ and BSG/SiO$_x$N$_y$ passivation

The passivation quality of PECVD BSG/SiN_z and also of

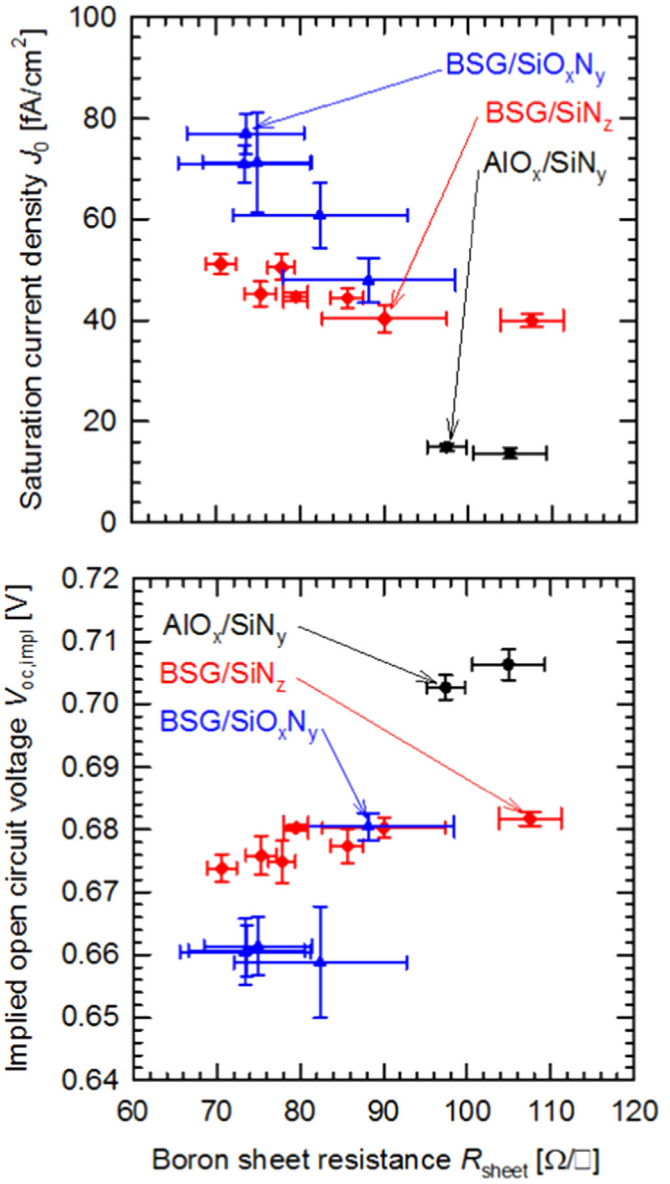

Fig. 4. J_0 and $V_{oc,\ impl.}$ for different PECVD BSG and ALD AlO_x passivation stacks on symmetrically boron diffused and passivated 15.6×15.6 cm^2 n-type wafers. (For interpretation of the references to color in this figure, the reader is referred to the web version of this article.)

BSG/SiO_xN_y stacks is evaluated and compared to a AlO_x/SiN_y passivation on symmetrically boron diffused planar n-type Cz wafers. The optimized, 40 nm-thin PECVD BSG boron diffusion source with $SiH_4/B_2H_6 = 8\%$ and the co-diffusion as described in Section 2.1 are applied. The measured saturation current density J_0 and the implied open circuit voltage $V_{oc,\ impl.}$ in dependence on the boron sheet resistance R_{sheet} are plotted in Fig. 4. The observed variation of R_{sheet} for the BSG/SiN_z diffused and passivated samples does not correlate with the applied capping layer thicknesses of either 120 nm or 180 nm SiN_z, however, we observe run to run variations in the PECVD tools.

Lowest J_0 values of (40 ± 1) fA/cm^2 and highest $V_{oc,\ impl.}$ values of (682 ± 1) mV are reached using a BSG/SiN_z stack (red diamonds) with a SiN_z thickness of 120 nm at a sheet resistance of (108 ± 4) Ω/□. For a SiO_xN_y capping layer (blue triangles), a minimum J_0 value of (48 ± 5) fA/cm^2 is reached for $R_{sheet} = (88 \pm 10)$ Ω/□, the measured standard deviations – especially in R_{sheet} – are significantly higher. We attribute this behaviour to a thickness inhomogeneity of the

Table 1
Measured IV parameters of the best co-diffused and of the best sequentially diffused reference *n*-PERT BJ cells obtained on a cell area of 239 cm^2 with 5 busbar layout.

Cell concept	V_{oc} (mV)	J_{sc} (mA/cm^2)	*FF* (%)	η (%)
n-PERT BJ co-diffused [12]	666	39.1	80.5	21.0[a]
n-PERT BJ reference [17]	674	39.3	80.0	21.2[a]

[a] Independently confirmed by Fraunhofer ISE Cal Lab.

PECVD SiO_xN_y layer that was deposited with a target thickness of 200 nm or 300 nm in the wafer centre but toward the wafer edges the thickness is about 10% thinner. For an AlO_x/SiN_y passivation stack (black squares), which is known to enable excellent surface passivation [20], especially on boron-diffused p^+ regions, only (14 ± 1) fA/cm^2 and up to (706 ± 2) mV are measured.

We confirm that a stack of PECVD BSG/SiN_z is showing promising passivation quality with the lowest reported saturation current densities of 40 fA/cm^2. Although the J_0 values are not as low as that of AlO_x/SiN_y, the BSG/SiN_z diffusion source might be kept on the rear side of *n*-PERT BJ cells to replace the AlO_x/SiN_y rear side passivation during cell fabrication reducing etching and saving deposition steps and thus significantly simplifying the cell process.

3.3. Solar cell results and efficiency gain analysis

Table 1 shows the measured IV parameters of the best co-diffused *n*-PERT BJ cell. The application of the PECVD BSG diffusion source and the co-diffusion process results in an independently confirmed conversion efficiency of 21.0% as published in [12]. The efficiency is almost as high as the 21.2% of the reference *n*-PERT BJ cells with separate $POCl_3$ and BBr_3 diffusions [17] despite the simplified process.

The experimentally extracted $R_{sheet,B}$, $J_{0,B}$ and $V_{oc,\ impl.}$ data measured on unmetallized test wafers that were processed in parallel with the 21.0% *n*-PERT BJ cell is summarized in Table 2. The boron doping from 40 nm PECVD BSG with SiH_4/B_2H_6=8% after passivation with AlO_x/SiN_y results in $J_{0,B}$ values of 21 fA/cm^2 compared to 24 fA/cm^2 for the BBr_3-diffused reference cell. The J_0 values reached on these samples are not as low as shown in Fig. 3 (red diamonds) because of the lower $R_{sheet,B}$ of 70 Ω/□ reached after a co-diffusion with slightly different process parameters. The $J_{0,P}$ after co-diffusion, that is measured on symmetrically P-diffused *p*-type Cz wafers, is about 50% higher compared to a separate $POCl_3$-diffusion resulting in a decreased V_{oc} for the co-diffused *n*-PERT BJ cells. For a passivation with a BSG/SiN_z stack, the $R_{sheet,B}$, $J_{0,B}$ and implied $V_{oc,B}$ data from Fig. 4 and the $R_{sheet,P}$, $J_{0,P}$ and implied $V_{oc,P}$ results measured on the *p*-type samples that were present in the same co-diffusion process are also listed in Table 2. The increased boron sheet resistance of 90 Ω/□ compared to 70 Ω/□ results from run to run variations in the PECVD tools, a PECVD BSG/SiN_z diffusion source with the same parameters (40 nm PECVD BSG with SiH_4/B_2H_6=8% capped with 120 nm SiN_z) is applied for both co-diffused cell concepts.

We perform two-dimensional device simulations applying the CoBo model [21] as implemented in the Quokka software [22]. The CoBo model uses the experimentally extracted R_{sheet} and J_0 data from Table 2 and further parameters given in [17] as input parameters. Important parameters are the measured wafer thickness of 151 μm and a wafer resistivity of 5.6 Ω cm. For the metallized regions, J_0 values of 400 fA/cm^2 for the Ag front contacts and of 320 fA/cm^2 for the Al rear contacts are applied. The simulated cell results are specified in Table 3. For the co-diffused and the reference cell with AlO_x/SiN_y rear side passivation, the simulated J_{sc} values match the experimental results listed in Table 1, but the V_{oc} values are overestimated in the simulations resulting in higher simulated *FF* and η compared to the experimental data. The simulated cell results for a BSG/SiN_z passivation show the same J_{sc} and *FF* results as with a AlO_x/SiN_y stack, but a reduced V_{oc} due to the higher $J_{0,B}$ of 40 fA/cm^2 instead of 21 fA/cm^2. According to the Quokka simulations, a conversion efficiency of 21.1% is to be expected, that may be overestimated by 0.2%$_{abs}$, as observed for the co-diffused *n*-PERT BJ cell efficiency. Hence, the slightly higher $J_{0,B}$ value of the BSG/SiN_z passivation compared to the AlO_x/SiN_y passivation translates into a 0.1%$_{abs}$ lower conversion efficiency. In summary, comparable cell results can be reached by the BSG/SiN_z passivation while realizing significant process simplifications.

Fig. 5 shows the results of a synergistic energy gain analysis (SEGA) [23] of the simulated *n*-PERT BJ cell applying co-diffusion and AlO_x/SiN_y rear side passivation. The SEGA quantifies all individual power losses of the PERT BJ solar cell by setting the respective simulation input parameter from its real value to an ideal value corresponding to an ideal silicon solar cell with 29.0% efficiency. Hence the simulated efficiency gains for the different loss mechanisms (grouped in resistance, optics and recombination) are determined. In addition, by deactivating groups of losses simultaneously, the interaction of loss mechanisms are taken into account and efficiency gains from these "synergistic" effects are identified. For more details on the SEGA analysis and the origin of the synergy contributions we refer to reference [24].

The largest gain (1.1%$_{abs}$) is possible when eliminating recombination in the non-metallized area of the phosphorus diffusion on the front side. In contrast, there is only a small gain of 0.1%$_{abs}$ possible when eliminating the recombination at the non-contacted boron diffusion. This demonstrates that the quality of our PECVD BSG boron diffusion is sufficiently high and reduces the efficiency of our cell by less than 0.1%. There is only a 0.1%$_{abs}$ gain from recombination in the bulk due to the used *n*-type silicon base material with a high bulk lifetime. Reducing recombination offers the largest potential for further cell improvements amounting in an ideal scenario to 1.5%$_{abs}$ from the sum of all individual recombination gains and a maximum improvement of 2.6%$_{abs}$ from synergistic effects if all recombination losses could be eliminated simultaneously. Through optical improvements, (2.2+0.1)%$_{abs}$ efficiency gain from the sum of all optical gains and from synergistic effects can be achieved while resistive improvements only contribute to 0.7%$_{abs}$.

Table 2
Experimentally R_{sheet}, J_0 and $V_{oc,\ impl.}$ results of the boron and phosphorus dopings of the best *n*-PERT BJ cells measured on symmetrically fabricated *n*-type Cz J_0-samples using $n_i = 8.6 \times 10^9\ cm^{-3}$ with an AlO_x/SiN_x or a BSG/SiN_z passivation and after firing.

Cell concept	$R_{sheet,B}$ (Ω/□)	$J_{0,B}$ (mA/cm^2)	impl. $V_{oc,B}$ (mV)	$R_{sheet,P}$ (Ω/□)	$J_{0,P}$ (mA/cm^2)	impl. $V_{oc,P}$ (mV)
n-PERT BJ co-diffused	70	21	697	92	87	668
n-PERT BJ co-diffused, BSG/SiN_z passivated	90	40	680	92	87	668
n-PERT BJ reference	100	24	707	155	46	670

Table 3
Simulated cell results for co-diffused and reference *n*-PERT BJ cells obtained on a cell area of 239 cm^2 with 5 busbar layout. Also simulated results for a co-diffused cell with a BSG/SiN_z rear side passivation instead of AlO_x/SiN_y are listed.

Cell concept	V_{oc} (mV)	J_{sc} (mA/cm^2)	*FF* (%)	η (%)
n-PERT BJ co-diffused	673	38.9	81.2	21.2
n-PERT BJ co-diffused, BSG/SiN_z passivated	669	38.9	81.1	21.1
n-PERT BJ reference	679	39.4	81.0	21.6

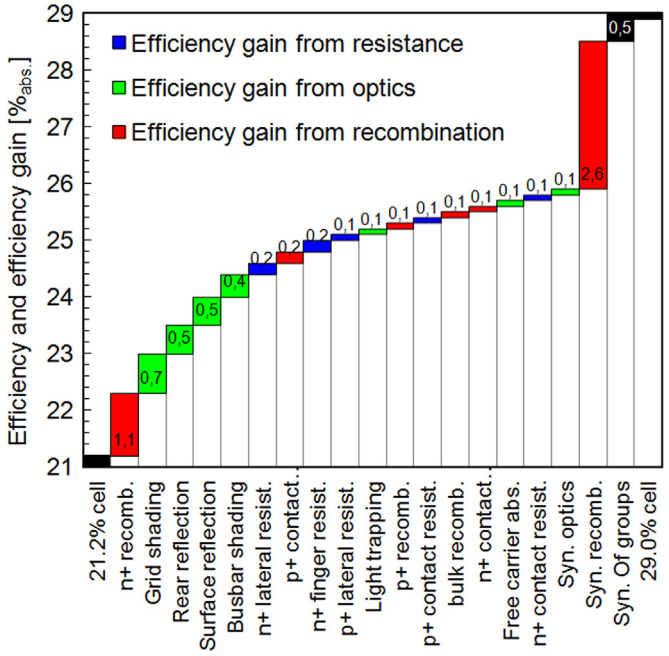

Fig. 5. Synergistic energy gain analysis (SEGA) results for the simulated 21.2%-efficient co-diffused *n*-PERT BJ cell with AlO_x/SiN_y rear side passivation.

4. Conclusions

We have demonstrated a record-high efficiency of 21.0% for a *n*-PERT BJ cell applying a optimized PECVD BSG/SiN_z diffusion source and a co-diffusion process. We obtained saturation current densities for the AlO_x/SiN_y passivated boron emitter down to 4.9 fA/cm^2. A SEGA proves the quality of our boron diffusion source and shows the optimization potential for the phosphorus diffusion that leads to the main possible efficiency gain from recombination of 1.1%$_{abs}$ The recombination in the phosphorus diffused FSF can be reduced by aiming for a higher P sheet resistance during $POCl_3$ co-diffusion comparable to R_{sheet} = 155 Ω/□ of the reference cell and thus reducing $J_{0,P}$ to values below 50 fA/cm^2, as could be reached during the $POCl_3$-diffusion of the reference cell.

Through a multifunctional use of the BSG/SiN_z as diffusion source and as rear side passivation instead of AlO_x/SiN_y, a further process simplification is possible so that LID-free screen-printed *n*-PERT BJ cells can be processed with a comparable process complexity as industrial *p*-PERC cells. We obtained lowest J_0 values of 40 fA/cm^2 for a BSG/SiN_z passivation with a 40 nm-thick PECVD BSG layer capped with a 120 nm-thick SiN_z layer. Device simulations show an only 0.1%$_{abs}$ reduced cell efficiency by keeping the BSG/SiN_z stack instead of depositing an AlO_x/SiN_y passivation layer stack and thus reducing dielectric etching step duration and saving deposition steps.

Acknowledgements

We thank Miriam Berger for *n*-PERT cell processing, Sarah Spätlich for diffusion optimization and David Sylla for laser processes. This work was funded by the German Federal Ministry for Economic Affairs and Energy under Grant 0325880A (PERC 2.0) and by the State of Lower Saxony.

References

[1] (International) Technology Roadmap for Photovoltaic (ITRPV), Results 2015, Seventh edition, March 2016.
[2] ⟨http://www.pv-magazine.com/news/details/beitrag/trina-solar-sets-efficiency-record-with-c-si-cell_100022472/#axzz41q0kJmq5⟩, (16.12.2015).
[3] J. Schmidt, Light-induced degradation in crystalline silicon solar cells, Solid State Phenom. 95–96 (2004) 187–196.
[4] T. Dullweber, C. Kranz, U. Baumann, R. Hesse, D. Walter, J. Schmidt, P. Altermatt, R. Brendel, Silicon wafer material options for highly efficient p-type PERC solar cells, in: Proceedings of the 39th IEEE PVSC, Tampa, FL, USA, 2013, pp. 3074–3078.
[5] J. Schmidt, K. Bothe, R. Bock, C. Schmiga, R. Krain, R. Brendel, N-type silicon – the better material choice for industrial high-efficiency solar cells?, in: Proceedings of the 22nd EUPVSEC, 2007, pp. 998–1001.
[6] A. Urueña, M. Aleman, E. Cornagliotti, A. Sharma, J. Deckers, M. Haslinger, L. Tous, R. Russell, J. John, Y. Yao, T. Söderström, F. Duerinckx, J. Szlufcik, Beyond 22% large area n-type silicon solar cells with front laser doping and a rear emitter, in: Proceedings of the 31th EUPVSEC, 2015, pp. 410–413.
[7] V. Mertens, S. Bordihn, A. Mohr, K. Petter, J.W. Müller, D.J.W. Jeong, R. Hao, T. Ravi, 21.4% efficient fully screen printed n-type solar cell on epitaxially grown silicon wafers with built-in boron rear side emitter, in: Proceedings of the 31st EUPVSEC, 2015, pp. 1000–1002.
[8] S. Bordihn et al., Status of industrial back junction n-type Si solar cell development, in: Proceedings of the 6th International Conference on Silicon Photovoltaics, Chambéry, France, 2016.
[9] P. Rothhardt, S. Meier, K. Jiang, A. Wolf, D. Biro, 19.9% efficient bifacial n-type solar cell produced by co-diffusion-COBIN, in: Proceedings of the 29th EUPVSEC, 2014, pp. 653–655.
[10] A. Frey, J. Engelhardt, S. Fritz, S. Gloger, G. Hahn, B. Terheiden, N-type bi-facial solar cells with boron emitters from doped PECVD layers, in: Proceedings of the 29th EUPVSEC, 2014, pp. 656–660.
[11] R. Cabal, B. Grange, L. Bounaas, R. Monna, N. Plassat, E. Pihan, Y. Veschetti, 20% PERT technology adapted to n-type mono-like silicon: simplified process and narrowed cell efficiency distribution, in: Proceedings of the 29th EUPVSEC, 2014, pp. 648–652.
[12] N. Wehmeier, B. Lim, A. Nowack, J. Schmidt, T. Dullweber, R. Brendel, 21.0%-efficient co-diffused screen printed n-type silicon solar cell with rear-side boron emitter, Phys. Status Solidi RRL 10 (2) (2016) 148–152.
[13] J. Engelhardt, A. Frey, S. Gloger, G. Hahn, B. Terheiden, Passivating boron silicate glasses for co-diffused high-efficiency n-type silicon solar cell application, Appl. Phys. Lett. 107 (2015) 042102.
[14] N. Wehmeier, B. Lim, A. Merkle, A. Tempez, S. Legendre, H. Wagner, A. Nowack, T. Dullweber, P. Pietro Altermatt, APECVD BSG diffusion sources for simplified high-efficiency n-PERT BJ and BJBC solar cells, IEEE JPV 6 (1) (2016) 119–125.
[15] N. Wehmeier, G. Schraps, H. Wagner, B. Lim, N.-P. Harder, P.P. Altermatt, Boron-doped PECVD silicon oxides as diffusion sources for simplified high-efficiency solar cell fabrication, in: Proceedings of the 28th EUPVSEC, 2013, pp. 1980–1984.
[16] H. Hannebauer, T. Dullweber, U. Baumann, T. Falcon, R. Brendel, 21.2%-efficient fineline-printed PERC solar cell with 5 busbar front grid, Phys. Status Solidi RRL 8 (8) (2014) 675–679.
[17] B. Lim, T. Brendemühl, T. Dullweber, R. Brendel, Loss analysis of n-type passivated emitter rear totally diffused back-junction silicon solar cells with efficiencies up to 21.2%, IEEE J. Photovolt. 6 (2) (2016) 447–453.
[18] D.E. Kane, R.M. Swanson, Measurement of the emitter saturation current by a contactless photoconductivity decay method, in: Proceedings of the 18th IEEE Photovoltaic Specialists Conference, 1985, pp. 578–583.
[19] M.A. Kessler, T. Ohrdes, B. Wolpensinger, R. Bock, N.-P. Harder, Characterisation and implications of the boron rich layer resulting from open-tube liquid source BBr3 boron diffusion processes, in: Proceedings of the 34th IEEE Photovoltaic Specialists Conference, 2009.
[20] J. Schmidt, B. Veith, R. Brendel, Effective surface passivation of crystalline silicon using ultrathin Al_2O_3 films and Al_2O_3/SiN_x stacks, Phys. Status Solidi RRL 3 (2009) 287–289.
[21] R. Brendel, Modeling solar cells with the dopant-diffused layers treated as conductive boundaries, Prog. Photovolt. Res. Appl. 20 (2012) 31–43.
[22] A. Fell, Quokka version 2: selective surface doping, luminescence modeling and data fitting, IEEE Trans. Electron Devices 60 (2) (2012) 733–738.
[23] J.H. Petermann, Prozessentwicklung & verlustanalysen für dünne monokristalline siliziumsolarzellen und deren prozessierung auf modullevel, Dissertation (2014).
[24] R. Brendel, T. Dullweber, R. Peibst, C. Kranz, A. Merkle, D. Walter, Breakdown of the efficiency gap to 29% based on experimental input data and modelling, Prog. Photovolt.: Res. Appl. (2015).